*Inorg. Chem.* **2008**, *47*, 29–41


# Experimental and Theoretical Comparison of Actinide and Lanthanide Bonding in $M[N(EPR_2)_2]_3$ Complexes (M = U, Pu, La, Ce; E = S, Se, Te; R = Ph, *i*Pr, H)

**Andrew J. Gaunt,*,† Sean D. Reilly,† Alejandro E. Enriquez,† Brian L. Scott,† James A. Ibers,‡ Perumal Sekar,‡ Kieran I. M. Ingram,§ Nikolas Kaltsoyannis,*,§ and Mary P. Neu*,†**

*Chemistry Division, Plutonium Manufacturing and Technology Division, Materials Physics and Applications Division, and Associate Directorate for Chemistry, Life, and Earth Sciences, Los Alamos National Laboratory, Los Alamos, New Mexico 87545, Department of Chemistry, Northwestern University, 2145 Sheridan Road, Evanston, Illinois 60208-3113, and Department of Chemistry, University College London, 20 Gordon Street, London WC1H 0AJ, United Kingdom*

Received August 14, 2007

Treatment of $M[N(SiMe_3)_2]_3$ (M = U, Pu (An); La, Ce (Ln)) with $NH(EPPh_2)_2$ and $NH(EPiPr_2)_2$ (E = S, Se), afforded the neutral complexes $M[N(EPR_2)_2]_3$ (R = Ph, *i*Pr). Tellurium donor complexes were synthesized by treatment of $MI_3(sol)_4$ (M = U, Pu; sol = py and M = La, Ce; sol = thf) with $Na(tmeda)[N(TePiPr_2)_2]$. The complexes have been structurally and spectroscopically characterized with concomitant computational modeling through density functional theory (DFT) calculations. The An–E bond lengths are shorter than the Ln–E bond lengths for metal ions of similar ionic radii, consistent with an increase in covalent interactions in the actinide bonding relative to the lanthanide bonding. In addition, the magnitude of the differences in the bonding is slightly greater with increasing softness of the chalcogen donor atom. The DFT calculations for the model systems correlate well with experimentally determined metrical parameters. They indicate that the enhanced covalency in the M–E bond as group 16 is descended arises mostly from increased metal d-orbital participation. Conversely, an increase in f-orbital participation is responsible for the enhancement of covalency in An–E bonds compared to Ln–E bonds. The fundamental and practical importance of such studies of the role of the valence d and f orbitals in the bonding of the f elements is emphasized.

## 1. Introduction

Two fundamental questions in f-element chemistry are, (1) to what extent do relativistic effects impact the coordination chemistry of these elements, and (2) what are the bonding differences between 4f and 5f ions of identical ionic radii? Addressing these questions is not only a necessity to acquire a comprehensive understanding of the fundamental electronic, structural, and bonding properties of the f elements but is also highly relevant to industrially important An(III)/Ln(III) (An = actinide, Ln = lanthanide) separations that are vital to the development of advanced nuclear fuel cycles and waste remediation.[1−16] In particular, the extent to which covalent contributions are important in f-metal bonding with

* To whom correspondence should be addressed. E-mail: gaunt@lanl.gov (A.J.G.), n.kaltsoyannis@ucl.ac.uk (N.K.), mneu@lanl.gov (M.P.N.).
† Los Alamos National Laboratory.
‡ Northwestern University.
§ University College London.

(1) Roger, M.; Barros, N.; Arliguie, T.; Thuéry, P.; Maron, L.; Ephritikhine, M. *J. Am. Chem. Soc.* **2006**, *128*, 8790.
(2) Miguirditchian, M.; Guillaneux, D.; Guillaumont, D.; Moisy, P.; Madic, C.; Jensen, M. P.; Nash, K. L. *Inorg. Chem.* **2005**, *44*, 1404.
(3) Roger, M.; Belkhiri, L.; Thuéry, P.; Arliguie, T.; Fourmigué, M.; Boucekkine, A.; Ephritikhine, M. *Organometallics* **2005**, *24*, 4940.
(4) Denecke, M. A.; Rossberg, A.; Panak, P. J.; Weigl, M.; Schimmelpfennig, B.; Geist, A. *Inorg. Chem.* **2005**, *44*, 8418.
(5) Mehdoui, T.; Berthet, J.-C.; Thuéry, P.; Ephritikhine, M. *Chem. Commun. (Cambridge)* **2005**, 2860.
(6) Mehdoui, T.; Berthet, J.-C.; Thuéry, P.; Salmon, L.; Rivière, E.; Ephritikhine, M. *Chem. Eur. J.* **2005**, *11*, 6994.
(7) Mehdoui, T.; Berthet, J.-C.; Thuéry, P.; Ephritikhine, M. *Eur. J. Inorg. Chem.* **2004**, 1996.
(8) Karmazin, L.; Mazzanti, M.; Bezombes, J.-P.; Gateau, C.; Pécaut, J. *Inorg. Chem.* **2004**, *43*, 5147.
(9) Choppin, G. R. *J. Alloys Compd.* **2002**, *344*, 55.
(10) Jensen, M. P.; Bond, A. H. *Radiochim. Acta* **2002**, *90*, 205.
(11) Berthet, J.-C.; Miquel, Y.; Iveson, P. B.; Nierlich, M.; Thuéry, P.; Madic, C.; Ephritikhine, M. *J. Chem. Soc., Dalton Trans.* **2002**, 3265.
(12) Jensen, M. P.; Bond, A. H. *J. Am. Chem. Soc.* **2002**, *124*, 9870.

10.1021/ic701618a CCC: $40.75 
Published on Web 11/20/2007

soft donor atoms remains unresolved, as does the role of the valence d and f orbitals. One approach to studying this topic is to crystallographically characterize complexes of 4f and 5f metal ions, of similar ionic radii, with soft-donor atom ligands and to use increasingly precise single-crystal X-ray diffraction data and computational bonding models to observe and provide rationale for subtle differences in M−L bond lengths, specifically to identify and understand differences in covalency.

Obvious functionalities to utilize for studies of covalency are An═L multiple bonds. The bonding of higher oxidation states (+VI and +V) of some of the early actinides (U, Np, Pu, and Am) is dominated by the linear actinyl cations[17] that contain the multiply bonded dioxo O═An═O moiety,[18] but no high oxidation states for the lanthanides exist for comparison with the actinyl ions. Multiple bonds in lower oxidation-state actinide ions (mostly U(IV)) occur with sterically bulky and inert stabilizing ligands such as $Cp^{*-}$ (pentamethylcyclopentadienide).[19] However, we are not aware of any isostructural comparisons of M═L multiple bonds between 4f and 5f complexes. This is probably a reflection of the dearth of M═L multiple bonds reported in f-element chemistry, particularly of An(III)═L multiple bonds. Therefore, we need to look to other functionalities and systems to assess covalency differences between An and Ln bonding.

Coordination chemistry studies that directly compare An and Ln bonding to soft donor atoms have been inspired to a large extent by solution Ln(III)/An(III) extraction, separation, and ion exchange experiments, which have demonstrated a preference of soft donor extractants for An(III) ions over Ln(III) ions.[10,12,15,20−23] Understanding the origin of the separation and extraction behaviors with soft donors is greatly aided by the synthesis and characterization of crystallizable molecular complexes containing soft-donor ligands, which allows structural and geometric data to be obtained that are vital for a combined experimental and computational investigation. A relatively small number of studies have observed shorter actinide−ligand than lanthanide−ligand bond lengths with soft-donor atom ligands in structurally similar complexes. For example, in the phosphite complexes $(MeC_5H_4)_3$-ML (M = U or Ce; L = $P(OCH_2)_3CEt$) the U−P distance is shorter than the Ce−P distance by 0.098 Å.[16] In the complexes $M(9\text{-ane}S_3)I_3(MeCN)_2$ (M = U, La; 9-ane$S_3$ = 1,4,7-trithiacyclononane) the average U−S distance is shorter than the average La−S distance by 0.0435 Å,[14] and in the complexes $M(tpza)I_3(thf)$ (M = U, La; tpza = tris[(2-pyrazinyl)methyl]amine) the average $U-N_{pyrazine}$ distance is shorter than the average $La-N_{pyrazine}$ distance by 0.048 Å.[13] The comparison of bonding in $M(SMes^*)_3$ (M = U, La; SMes* is a "supermesityl" thiolate ligand) complexes revealed a U−S distance that is shorter than the La−S distance by an average value of 0.025 Å;[1] this represents a rare example in which homoleptic 4f/5f complexes with soft donors have been compared. Interestingly, Jensen and Bond conducted an EXAFS solution study to look for differences in bond lengths in trivalent Am, Cm, Nd, and Sm complexes with dithiophosphinic acids, which have shown exceptional selectivity for Am(III) over Eu(III) in liquid−liquid extraction studies.[12] However, in that study there was no evidence from the EXAFS data of shortened An−S bonds relative to Ln−S bonds. It may well be that the observed extraction behavior still was the result of increased covalency in the An−S bonds relative to the Ln−S bonds but that the bond length differences were too small to be observed experimentally. Therefore, to be able to observe bond length differences resulting from covalency, it may be necessary to use model soft-chalcogen donor complexes judiciously chosen to maximize covalent character and then to extrapolate those results to more applied solvent extraction systems.

Our approach to elucidating differences in covalency between An(III) and Ln(III) bonding, as described here, is to undertake an experimental and theoretical comparison of homoleptic, structurally similar An(III) and Ln(III) complexes in which two important factors are explored: (1) The electronegativity (or softness) of the ligand donor atom is varied in order to test the hypothesis that An(III) ions have greater covalency in their bonding with soft donor ligands than do Ln(III) ions of identical ionic radii and that the difference in covalency is more pronounced the softer the donor atom. (2) The positive charge density of the 4f- and 5f-metal ions is varied to study the effect that the lanthanide/actinide contraction has upon bonding differences, in order to test the hypothesis that, as the f-element series is traversed, the potential for any covalency in the bonding decreases. In this respect, we recently communicated the syntheses and molecular structures of $M[N(TeP\textit{i}Pr_2)_2]_3$ (M = U, La)[24] and $U[N(EPPh_2)_2]_3$ (E = S, Se)[25] complexes along with preliminary computational results on the La, U, and Pu systems[26]


(13) Mazzanti, M.; Wietzke, R.; Pécaut, J.; Latour, J.-M.; Maldivi, P.; Remy, M. *Inorg. Chem.* **2002**, *41*, 2389.
(14) Karmazin, L.; Mazzanti, M.; Pécaut, J. *Chem. Commum. (Cambridge)* **2002**, 654.
(15) Choppin, G. R.; Nash, K. L. *Radiochim. Acta* **1995**, *70−1*, 225.
(16) Brennan, J. G.; Stults, S. D.; Andersen, R. A.; Zalkin, A. *Organometallics* **1988**, *7*, 1329.
(17) See, for example: (a) Burns, C. J.; Neu, M. P.; Boukhalfa, H.; Gutowski, K. E.; Bridges, N. J.; Rogers, R. D. in *Comprehensive Coordination Chemistry II*, Vol. 3; McCleverty, J. A., Meyer, T. J., Eds.; Elsevier Pergamon: Amsterdam, 2004; p 189. (b) Katz, J. J.; Seaborg, G. T.; Morss, L. R. *The Chemistry of the Actinide Elements*, Vols. 1 and 2, 2nd ed.; Chapman and Hall: New York, 1986.
(18) Denning, R. G. *Struct. Bonding (Berlin)* **1992**, *79*, 215.
(19) See, for example: (a) Jantunen, K. C.; Burns, C. J.; Castro-Rodriguez, I.; Da Re, R. E.; Golden, J. T.; Morris, D. E.; Scott, B. L.; Taw, F. L.; Kiplinger, J. L. *Organometallics* **2004**, *23*, 4682. (b) Arney, D. S. J.; Schnabel, R. C.; Scott, B. L.; Burns, C. J. *J. Am. Chem. Soc.* **1996**, *118*, 6780. (c) Arney, D. S. J.; Burns, C. J. *J. Am. Chem. Soc.* **1995**, *117*, 9448. (d) Cramer, R. E.; Maynard, R. B.; Paw, J. C.; Gilje, J. W. *J. Am. Chem. Soc.* **1981**, *103*, 3589.
(20) Hagström, I.; Spjuth, L.; Enarsson, Å.; Liljenzin, J. O.; Skålberg, M.; Hudson, M. J.; Iveson, P. B.; Madic, C.; Cordier, P. Y.; Hill, C.; Francois, N. *Solvent Extr. Ion Exch.* **1999**, *17*, 221.
(21) Zhu, Y. *Radiochim. Acta* **1995**, *68*, 95.
(22) Musikas, C.; Cuillerdier, C.; Livet, J.; Forchioni, A.; Chachaty, C. *Inorg. Chem.* **1983**, *22*, 2513.
(23) Diamond, R. M.; Street, K., Jr.; Seaborg, G. T. *J. Am. Chem. Soc.* **1954**, *76*, 1461.
(24) Gaunt, A. J.; Scott, B. L.; Neu, M. P. *Angew. Chem., Int. Ed.* **2006**, *45*, 1638.
(25) Gaunt, A. J.; Scott, B. L.; Neu, M. P. *Chem. Commun. (Cambridge)* **2005**, 3215.
(26) Ingram, K. I. M.; Kaltsoyannis, N.; Gaunt, A. J.; Neu, M. P. *J. Alloys Compd.* **2007**, *444−445*, 369.

that demonstrated the potential of imidodiphosphinochalcogenide ligand systems to facilitate a systematic study of An(III) vs Ln(III) covalency. Here we report a much more comprehensive structural and spectroscopic characterization of $M[N(EPPh_2)_2]_3$ (M = U, Pu, La, Ce; E = S, Se) and $M[N(EP{\it i}Pr_2)_2]_3$ (M = U, Pu, La, Ce; E = S, Se, Te), together with density functional theory studies of $M[N(EPH_2)_2]_3$ (M = U, Pu, La, Ce; E = O, S, Se, Te) models for the *i*Pr systems. We decided to focus our computational efforts on the six-coordinate bidentate systems, so as to remove the potentially complicating effects of M(III)−N bonding in the nine-coordinate tridentate systems. It is noteworthy that undertaking a study involving nonaqueous coordination chemistry of molecular plutonium compounds is particularly challenging owing to the difficulty of handling high specific activity transuranic radionuclides and the paucity of well-characterized precursors. Nevertheless, such studies are important if we are to understand the effect of the f-element contraction in these complexes.

## 2. Experimental Section

**2.1. Syntheses. Caution!** $^{239}Pu$ is a high specific-activity α-particle-emitting radionuclide. This research was conducted in a radiological facility with appropriate analyses of hazards and implementation of controls for the safe handling and manipulation of radioactive materials.

α-phase plutonium metal pieces of weapons-grade isotopic composition and uranium turnings (depleted in $^{235}U$) were obtained internally from Los Alamos National Laboratory. All reactions were performed in an MBraun Labmaster 130 helium atmosphere drybox. Diethyl ether, toluene, hexanes, and tetrahydrofuran (THF) were dried with the use of activated alumina columns (A2, 12 32, Purify). Other solvents were purchased in anhydrous grade from Aldrich. All solvents were stored over a 1:1 mixture of 3 and 4 Å molecular sieves before use. Infrared spectra were obtained as Nujol mulls between KBr plates on a Nicolet Magna-IR 560 spectrometer equipped with a DTGS detector. $^1H$ NMR spectra were referenced to residual protio resonances, and $^{31}P$ NMR spectra were referenced to external 85% $H_3PO_4$. All NMR spectra were obtained on samples in 4 mm Teflon NMR tube liners inserted into 5 mm NMR tubes in order to multiply contain the radioactive samples. NMR spectra were recorded at ambient temperature on a Bruker Avance 300 MHz spectrometer. Electronic absorption spectra were recorded on a Varian Cary 6000i UVvis/near-IR spectrophotometer. Elemental analyses were performed by the Micro-Mass facility at the University of California at Berkeley, Berkeley, CA. $U[N(SiMe_3)_2]_3$ was prepared according to the literature,[27] and $Pu[N(SiMe_3)_2]_3$ was prepared by a modification of a literature procedure.[27] $UI_3(py)_4$ and $PuI_3(py)_4$ were prepared according to the literature.[27] $LaI_3(thf)_4$ and $CeI_3(thf)_4$ were prepared by stirring anhydrous $LaI_3$ and $CeI_3$ in THF overnight and collecting the resulting powders.

**2.1.1. U[N(SPPh$_2$)$_2$]$_3$·toluene (1).** This compound was prepared as previously described.[25]

**2.1.2. La[N(SPPh$_2$)$_2$]$_3$·toluene (2).** $NH(SPPh_2)_2$ (0.0448 g, 0.100 mmol) was dissolved in THF (1.5 mL) and filtered through a glass fiber filter circle. $La[N(SiMe_3)_2]_3$ (0.0200 g, 0.032 mmol) was dissolved in toluene (1.5 mL), filtered and carefully layered on top of the ligand THF solution. Crystals of **2** precipitated from solution over several days. The mother liquor was pipetted away; the crystals were collected and dried in vacuo to give a white powder (0.0362 g, 76% yield). $^{31}P\{^1H\}$ NMR: ($CD_2Cl_2$): $\delta$ 42.6. IR (KBr, Nujol, $cm^{-1}$): 1199(s), 1179(m), 1156(m), 1070(m), 1026(w), 999(w), 977(w), 969(w), 918(w), 756(w), 744(m), 739(m), 724(s), 715(m), 707(w), 693(s), 626(w), 619(w), 609(w), 596(s), 513(s), 493(m), 470(m). Anal. Calcd for $C_{79}H_{68}N_3P_6S_6La$: C, 60.19; H, 4.35; N, 2.67. Found: C, 60.46; H, 4.27; N, 2.61.

**2.1.3. Pu[N(SPPh$_2$)$_2$]$_3$·toluene(3).** This compound was prepared as for **2** using $NH(SPPh_2)_2$ (0.0187 g, 0.042 mmol) and $Pu[N(SiMe_3)_2]_3$ (0.0100 g, 0.014 mmol) to yield crystalline **3**, which was harvested as a green powder after drying (0.0173 g, 79% yield). $^{31}P\{^1H\}$ NMR ($C_4D_8O$) (prepared in situ because of the low solubility of **3**): $\delta$ −47.11 (complex **3**), 52.06 (free ligand). UV/vis/near-IR (solution of **3** prepared in situ in THF) ($\lambda_{max}$, nm): 247, 299, 351, 520, 566, 578, 612, 674, 787, 826, 920, 1036, 1136, 1437, 1531.

**2.1.4. Ce[N(SPPh$_2$)$_2$]$_3$·toluene (4).** The compound was prepared as for **2** using $NH(SPPh_2)_2$ (0.0672 g, 0.149 mmol) and $Ce[N(SiMe_3)_2]_3$ (0.0300 g, 0.048 mmol) to yield crystalline **4**, which was harvested as a pale yellow/green powder after drying (0.0426 g, 59% yield). $^{31}P\{^1H\}$ NMR ($CD_2Cl_2$): $\delta$ 4.92. IR (KBr, Nujol) ($cm^{-1}$): 1200(s), 1178(s), 1156(m), 1101(m), 1069(w), 1026(w), 999(w), 977(w), 967(w), 918(w), 894(w), 843(w), 773(w), 756(m), 744(m), 739(m), 724(s), 712(m), 707(w), 693(s), 626(w), 619(w), 596(s), 513(s), 492(m), 470(m). Anal. Calcd for $C_{79}H_{68}N_3P_6S_6Ce$: C, 60.14; H, 4.34; N, 2.66. Found: C, 60.86; H, 4.49; N, 2.54.

**2.1.5. U[N(SePPh$_2$)$_2$]$_3$·C$_6$D$_6$ (5).** This compound was prepared as previously described.[25]

**2.1.6. La[N(SePPh$_2$)$_2$]$_3$·toluene (6).** This compound was prepared as for **2** using $NH(SePPh_2)_2$ (0.0540 g, 0.099 mmol) and $La[N(SiMe_3)_2]_3$ (0.0200 g, 0.032 mmol) to yield crystalline **6**, which was harvested as a white powder after drying (0.0392 g, 69% yield). $^{31}P\{^1H\}$ NMR: ($CD_2Cl_2$): $\delta$ 33.6 IR (KBr, Nujol; $cm^{-1}$): 1185(m), 1165(s), 1154(s), 1098(m), 1069(m), 1024(m), 998(w), 977(w), 967(w), 918(w), 843(w), 755(m), 743(m), 738(m), 721(s), 711(m), 690(s), 654(m), 618(w), 562(s), 547(m), 541(m), 507(s), 481(m), 468(w), 453(w). Anal. Calcd for $C_{79}H_{68}N_3P_6Se_6La$: C, 51.07; H, 3.69; N, 2.26. Found: C, 51.60; H, 3.50; N, 2.22.

**2.1.7. Pu[N(SePPh$_2$)$_2$]$_3$·toluene (7).** This compound was prepared as for **2** using $NH(SePPh_2)_2$ (0.0226 g, 0.042 mmol) and $Pu[N(SiMe_3)_2]_3$ (0.0100 g, 0.014 mmol) to yield crystalline **7**, which was harvested as a green powder after drying (0.0155 g, 60% yield). $^{31}P\{^1H\}$ NMR ($C_4D_8O$): $\delta$ −59.18 (complex **7**), 51.97 (free ligand). Peaks integrate with the ratio 7:1. UV/vis/near-IR (solution of **7** in THF) ($\lambda_{max}$, nm): 245, 326, 523, 576, 611, 618, 675, 797, 811, 828, 917, 932, 1041, 1061, 1116, 1127, 1141, 1164, 1447, 1514.

**2.1.8. Ce[N(SePPh$_2$)$_2$]$_3$·toluene (8).** This compound was prepared as for **2** using $NH(SePPh_2)_2$ (0.0807 g, 0.149 mmol) and $Ce[N(SiMe_3)_2]_3$ (0.0300 g, 0.048 mmol) to yield crystalline **8**, which was harvested as a pale green powder after drying (0.0528 g, 62% yield). $^{31}P\{^1H\}$ NMR ($CD_2Cl_2$): $\delta$ −8.34. IR (KBr, Nujol; $cm^{-1}$): 1185(w), 1167(s), 1154(s), 1098(m), 1071(w), 1025(w), 998(w), 976(w), 969(w), 936(w), 918(w), 893(w), 850(w), 772(w), 755(w), 743(w), 738(m), 721(s), 690(m), 654(m), 618(w), 561(m), 547(m), 540(w), 530(w), 508(m), 481(w), 418(w). Anal. Calcd for $C_{79}H_{68}N_3P_6Se_6Ce$: C, 51.04; H, 3.69; N, 2.26. Found: C, 51.70; H, 3.90; N, 2.21.

**2.1.9. U[N(SP*i*Pr$_2$)$_2$]$_3$ (9).** $U[N(SiMe_3)_2]_3$ (0.0500 g, 0.070 mmol) was dissolved in THF (6 mL). $NH(SP{\it i}Pr_2)_2$ (0.0653 g, 0.208 mmol) was dissolved in THF (2 mL) and added dropwise to the U-containing solution. The resulting purple solution was stirred overnight. The solution was filtered, and the solvent was removed

(27) Avens, L. R.; Bott, S. G.; Clark, D. L.; Sattelberger, A. P.; Watkin, J. G.; Zwick, B. D. *Inorg. Chem.* **1994**, *33*, 2248.

in vacuo to yield a purple powder, which was dried in vacuo (0.0642 g, 79% yield). Crystals suitable for X-ray diffraction were obtained from a THF/hexanes solution of **9** stored at −35 °C for several days. $^{31}P\{^1H\}$ NMR ($C_6D_6$): $\delta$ −525.1. IR (KBr, Nujol; $cm^{-1}$): 1266(s), 1230(s), 1169(m), 1159(m), 1096(w), 1080(m), 1040(w), 1029(m), 974(m), 933(m), 920(w), 885(m), 850(m), 775(m), 722-(s), 677(m), 656(m), 628(w), 563(w), 550(w), 539(w), 504(w), 489-(w), 474(w). UV/vis/near-IR (solution of **9** in THF) ($\lambda_{max}$, nm): 302(sh), 474(sh), 541(sh), 571, 616(sh), 644(sh), 675(sh), 710(sh), 779(sh), 928, 1097, 1210, 1250. Anal. Calcd for $C_{36}H_{84}N_3P_6S_6U$: C, 36.79; H, 7.20; N, 3.58. Found: C, 37.81; H, 7.38; N, 3.47.

**2.1.10. La[N(SP*i*Pr$_2$)$_2$]$_3$ (10).** La[N(SiMe$_3$)$_2$]$_3$ (0.0300 g, 0.048 mmol) was dissolved in THF (5 mL). NH(SP*i*Pr$_2$)$_2$ (0.0456 g, 0.145 mmol) was dissolved in THF (2 mL) and added dropwise to the La-containing solution. The resulting colorless solution was stirred overnight, the volume was then reduced in vacuo to 1 mL, and $Et_2O$ (5 mL) was added with shaking. The clear, colorless solution was stored at −35 °C for several days to give a white crystalline solid, which was dried in vacuo (0.0350 g, 67% yield). Crystals suitable for X-ray diffraction were obtained from a THF solution of **10** layered with $Et_2O$ and stored at −35 °C for several days. $^1H$ NMR ($C_6D_6$): $\delta$ 2.25 (m, 12H; C*H*(CH$_3$)$_2$), 1.38, 1.23 (m, 72H; CH(C*H*$_3$)$_2$). Less intense peaks were also observed for the minor free ligand component. $^{31}P\{^1H\}$ NMR ($C_6D_6$): $\delta$ 64.31 (complex **10**), 86.76 (free ligand). Peaks integrated with the ratio 12.9:1. IR (KBr, Nujol; $cm^{-1}$): 1268(s), 1232(s), 1162(m), 1096(w), 1080-(m), 1040(w), 1026(m), 974(m), 931(m), 884(s), 773(s), 722(s), 677(m), 656(s), 630(w), 563(w), 551(w), 540(w), 506(w), 489(m), 475(w), 419(m), 413(m). Anal. Calcd for $C_{36}H_{84}N_3P_6S_6La$: C, 40.18; H, 7.87; N, 3.90. Found: C, 40.53; H, 7.97; N, 3.91.

**2.1.11. Pu[N(SP*i*Pr$_2$)$_2$]$_3$ (11).** Pu[N(SiMe$_3$)$_2$]$_3$ (0.0246 g, 0.034 mmol) was dissolved in THF (5 mL), and NH(SP*i*Pr$_2$)$_2$ (0.0321 g, 0.102 mmol) was added. The solution was stirred overnight and then was filtered to give a green filtrate. $Et_2O$ (1 mL) was added with shaking, and the mixture was stored at −35 °C for several days to give green crystals, which were dried in vacuo (0.0162 g, 40% yield). $^1H$ NMR ($C_6D_6$): $\delta$ 2.20 (s, 12H; C*H*(CH$_3$)$_2$), 1.32, 1.22 (s, 72H; CH(C*H*$_3$)$_2$). $^{31}P\{^1H\}$ NMR ($C_6D_6$): $\delta$ −1.40. UV/vis/near-IR (solution of **11** in benzene) ($\lambda_{max}$, nm): 286, 299(sh), 321(sh), 345(sh), 392, 526, 578, 608, 619, 680, 801, 823, 915, 1051, 1130, 1139, 1149, 1450.

**2.1.12. Ce[N(SP*i*Pr$_2$)$_2$]$_3$ (12).** Ce[N(SiMe$_3$)$_2$]$_3$ (0.0150 g, 0.024 mmol) was dissolved in THF (5 mL), and NH(SP*i*Pr$_2$)$_2$ (0.0227 g, 0.072 mmol) was added and the solution stirred overnight. The resultant green solution was filtered, and then $Et_2O$ (1 mL) was added with shaking. The mixture was stored at −35 °C for several days to give a few green crystals, which were suitable for X-ray diffraction.

**2.1.13. U[N(SeP*i*Pr$_2$)$_2$]$_3$ (13).** U[N(SiMe$_3$)$_2$]$_3$ (0.0500 g, 0.070 mmol) was dissolved in THF (6 mL). NH(SeP*i*Pr$_2$)$_2$ (0.0850 g, 0.209 mmol) was dissolved in THF (2 mL) and added dropwise to the U-containing solution. The resultant purple solution was stirred overnight. The solution was filtered, and the solvent was removed in vacuo to yield a purple powder, which was dried in vacuo (0.0771 g, 76% yield). Crystals suitable for X-ray diffraction were obtained from a THF/hexanes solution of **13** stored at −35 °C for several days. $^{31}P\{^1H\}$ NMR ($C_6D_6$): $\delta$ −573.9. IR (KBr, Nujol; $cm^{-1}$): 1262(m), 1256(m), 1230(s), 1162(w), 1097(w), 1081(w), 1040(w), 1028(m), 973(w), 933(m), 905(w), 885(m), 850(m), 764(w), 722-(m), 682(w), 671(m), 632(s), 604(w), 519(w), 509(w), 474(w), 418-(w). UV/vis/near-IR (solution of **13** in THF) ($\lambda_{max}$, nm): 482(sh), 538, 579, 658(sh), 783(sh), 832, 935, 1073, 1235. Anal. Calcd for $C_{36}H_{84}N_3P_6Se_6U$: C, 29.68; H, 5.81; N, 2.88. Found: C, 29.38; H, 5.65; N, 2.74.

**2.1.14. La[N(SeP*i*Pr$_2$)$_2$]$_3$ (14).** La[N(SiMe$_3$)$_2$]$_3$ (0.0300 g, 0.048 mmol) was dissolved in THF (5 mL). NH(SeP*i*Pr$_2$)$_2$ (0.0591 g, 0.145 mmol) was dissolved in THF (2 mL) and added dropwise to the La-containing solution. The resulting colorless solution was stirred overnight, the volume was reduced in vacuo to 1 mL, and $Et_2O$ (5 mL) was added with shaking. The resultant clear, colorless solution was stored at −35 °C for several days to give a white crystalline solid, which was dried in vacuo (0.0483 g, 72% yield). Single crystals suitable for X-ray diffraction were obtained from a THF solution of **14** layered with $Et_2O$ and stored at −35 °C for several days. $^{31}P\{^1H\}$ NMR ($C_6D_6$): $\delta$ 56.78. $^1H$ NMR ($C_6D_6$): $\delta$ 2.12 (m, 12H; C*H*(CH$_3$)$_2$), 1.29 (m, 72H; CH(C*H*$_3$)$_2$). IR (KBr, Nujol; $cm^{-1}$): 1268(m), 1231(m), 1182(w), 1171(m), 1158(m), 1098(w), 1080(m), 1040(w), 1023(m), 974(m), 933(m), 885(m), 761(m), 722-(s), 682(w), 669(m), 630(s), 604(w), 519(w), 508(w), 473(m). Anal. Calcd for $C_{36}H_{84}N_3P_6Se_6La$: C, 31.85; H, 6.24; N, 3.01. Found: C, 31.93; H, 6.27; N, 3.06.

**2.1.15. Pu[N(SeP*i*Pr$_2$)$_2$]$_3$ (15).** Pu[N(SiMe$_3$)$_2$]$_3$ (0.0108, 0.015 mmol) was dissolved in THF (5 mL), and NH(SeP*i*Pr$_2$)$_2$ (0.0183 g, 0.045 mmol) was added. The solution was stirred overnight and was filtered to give a green filtrate, and then the solvent was removed in vacuo. The green powder was dissolved in toluene (1.5 mL), filtered, then layered with hexanes, and stored at −35 °C for several days to give green crystals, which were dried in vacuo (0.0078 g, 36% yield). $^1H$ NMR ($C_6D_6$): $\delta$ 2.23 (m, 12H; C*H*(CH$_3$)$_2$), 1.30 (s, 72H; CH(C*H*$_3$)$_2$). $^{31}P\{^1H\}$ NMR ($C_6D_6$): $\delta$ −20.06. UV/vis/near-IR (solution of **15** in benzene) ($\lambda_{max}$, nm): 298, 330, 414, 529, 556, 577, 608, 618, 683, 802, 826, 914, 1053, 1086, 1149, 1452.

**2.1.16. U[N(TeP*i*Pr$_2$)$_2$]$_3$ (16).** This compound was prepared as previously described.[24]

**2.1.17. La[N(TeP*i*Pr$_2$)$_2$]$_3$ (17).** This compound was prepared as previously described.[24]

**2.1.18. Pu[N(TeP*i*Pr$_2$)$_2$]$_3$ (18).** PuI$_3$(py)$_4$ (0.0148 g, 0.016 mmol) was suspended in $Et_2O$ (5 mL), and Na(tmeda)[N(TeP*i*Pr$_2$)$_2$] in $Et_2O$ (0.0307 g, 0.047 mmol) (2.5 mL) was added (tmeda = tetramethylethylenediamine). An orange/red suspension formed immediately. The suspension was stirred for 20 min and then stored overnight at −35 °C to allow the solid to settle to the bottom of the vial. The mother liquor was pipetted away, and the solid was dried in vacuo. Toluene (5 mL) was added to the solid, the solution filtered, and $Et_2O$ (10 mL) was added to the filtrate with shaking. The resultant solution was stored at −35 °C for several days to give a red microcrystalline solid, which was dried in vacuo (0.0119 g, 43% yield). Single crystals suitable for X-ray diffraction were obtained from a THF/$Et_2O$ solution of **18** stored at −35 °C for several days. $^1H$ NMR ($C_7D_8$): $\delta$ 1.97 (m, 12H; C*H*(CH$_3$)$_2$), 1.19 (s, 72H; CH(C*H*$_3$)$_2$). $^{31}P\{^1H\}$ NMR ($C_7D_8$): $\delta$ −62.22. UV/vis/near-IR (solution of **18** in toluene) ($\lambda_{max}$, nm): 467(sh), 579, 620, 685, 804, 829, 916, 1057, 1087(sh), 1148, 1465.

**2.1.19. Ce[N(TeP*i*Pr$_2$)$_2$]$_3$ (19).** CeI$_3$(THF)$_4$ (0.0300 g, 0.037 mmol) was suspended in $Et_2O$ (5 mL). Na(tmeda)[N(TeP*i*Pr$_2$)$_2$] (0.0720 g, 0.111 mmol) was dissolved in $Et_2O$ (2.5 mL) and added dropwise to the Ce-containing solution to afford a salmon-pink colored suspension, that was stirred for 20 min and then stored at −35 °C to allow the solid to settle to the bottom of the vial. The mother liquor was pipetted away, and the solid was dried in vacuo. Toluene (3 mL) was added to the solid, the solution filtered, and $Et_2O$ (10 mL) added to the filtrate with shaking. The resultant solution was stored at −35 °C for several days to give a pink-red

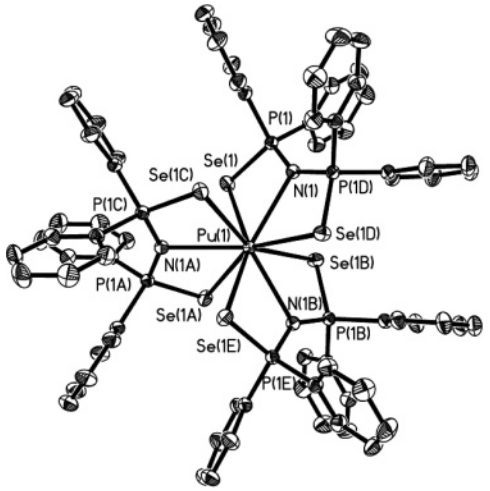


**Figure 1.** Thermal ellipsoid plot (at the 50% probability level) of the structure of $Pu[N(SePPh_2)_2]_3$ (**7**), with the H atoms and lattice toluene molecule omitted for clarity. The complexes **1**−**6** and **8** have identical connectivity.

microcrystalline solid, which was dried in vacuo (0.0221 g, 36% yield). Single crystals suitable for X-ray diffraction were obtained from a THF/$Et_2O$ solution of **19** stored at −35 °C for several days. $^1$H NMR ($C_7D_8$): $\delta$ 0.18 (s, 12H; C*H*($CH_3$)$_2$), −0.06, −0.81 (d, 72H; CH(C*H*$_3$)$_2$). $^{31}$P{$^1$H} NMR ($C_7D_8$): $\delta$ −9.98. IR (KBr, Nujol; cm$^{-1}$): 1275(m), 1227(m), 1202(m), 1181(w), 1171(w), 1157(m), 1097(w), 1077(m), 1033(w), 1018(m), 974(m), 932(m), 881(m), 772(w), 723(s), 694(m), 659(m), 635(m), 609(m), 597(m), 510-(m), 471(m). Anal. Calcd for $C_{36}H_{84}N_3P_6Te_6Ce$: C, 26.20; H, 5.13; N, 2.55. Found: C, 26.55; H, 5.06; N, 2.48.

**2.2. Crystallographic Data Collection and Refinement.** Each Pu-containing crystal was coated with Paratone−N and then mounted inside a 0.5 mm capillary. The capillaries were sealed with wax, and their external surfaces were coated with a thin film of acrylic dissolved in ethyl acetate (Hard as Nails nail polish) to provide appropriate containment of the radioactive material. Otherwise, non-Pu-containing crystals were mounted in Nylon cryoloops from Paratone−N oil under an argon-gas flow. The data for **5** [25] and **12** were collected on a Bruker P4/CCD diffractometer at 203 K with the use of a Bruker LT-2 temperature device. The instrument was equipped with a sealed, graphite-monochromatized Mo K$\alpha$ X-ray source ($\lambda$ = 0.710 73 Å). A hemisphere of data was collected using $\omega$ scans, with 30 s frame exposures and 0.3° frame widths at 203(2) K. The data for all the other crystals were collected on a Bruker SMART APEX II CCD X-ray diffractometer with a KRYO-FLEX liquid nitrogen vapor cooling device at 141(2) K. The instrument was equipped with a graphite-monochromatized Mo K$\alpha$ X-ray source ($\lambda$ = 0.710 73 Å), with MonoCap X-ray source optics. A hemisphere of data was collected using $\omega$ scans, with 5 s frame exposures at 0.3° frame widths. Data collection and initial indexing and cell refinement were handled with APEX II[28] software. Frame integration, including Lorentz−polarization corrections and final cell parameter calculations, were carried out using SAINT+[29] software. The data were corrected for absorption with the SADABS[30] program. Decay of reflection intensity was monitored via analysis of redundant frames. Each structure was solved using direct methods and difference Fourier techniques. All hydrogen-atom positions were idealized and rode on the atoms to which they were attached to. All non-hydrogen atoms were refined anisotropically. Structure solution, refinement, graphics, and creation of publication materials were performed using SHELXTL.[31] Further details may be found in the Supporting Information.

**2.3. Computational Details.** All calculations were carried out using gradient-corrected density functional theory, as implemented in the Gaussian (G03)[32] and Amsterdam Density Functional (ADF)[33] quantum chemical codes. Spin-unrestricted calculations were performed on all Ln and An complexes to account for the formal $f^n$ configurations of each Ln(III) and An(III) ion with the exception of the formally $f^0$ La(III) ion, on which spin-restricted calculations were performed.

**2.3.1. G03.** The GGA functional PBE[34,35] was used for all G03 calculations. (14s 13p 10d 8f)/[10s 9p 5d 4f] segmented valence basis sets with Stuttgart−Bonn variety[36] relativistic effective core potentials (RECPs) were used for the actinides, and a (14s 13p 10d 8f)/[10s 8p 5d 4f] segmented valence basis set with a Stuttgart−Bonn RECP[36] was used for each lanthanide. 6-31G* basis sets were used for the O, S, Se, N, and P atoms, and the smaller 6-31G set was used for H. Te was described with a (4s 5p)/[2s 3p] Stuttgart basis set[37] augmented to (4s 5p 7d)/[2s 3p 3d] with STO-3G* [38,39] polarization functions (for consistency, as 6-31G* includes polarization functions on O, S, and Se); a Stuttgart RECP was also used for Te.[37] The validity of this augmented Te basis set was checked by constructing an analogous Se basis set—a Stuttgart (4s 5p)/[2s 3p] augmented to (4s 5p 4d)/[2s 3p 2d]—and performing test geometry optimizations on $[M(N(SePH_2)_2)_3]$ for M = La, U; similar geometries were found with both methods. The default values for the integration grid ("fine") and the convergence criteria were used for all La, Ce, and U geometry optimizations (maximum force = $4.5 \times 10^{-4}$ au Å$^{-1}$; SCF = $10^{-8}$). The Pu calculations were more problematic, and the following convergence criteria were achieved: $[Pu(N(OPH_2)_2)_3]$ (maximum force = $7 \times 10^{-4}$ au Å$^{-1}$; SCF = $10^{-7}$), $[Pu(N(SPH_2)_2)_3]$ (maximum force = $8 \times 10^{-4}$ au Å$^{-1}$; SCF = $10^{-5}$), $[Pu(N(SePH_2)_2)_3]$ (maximum force = $5 \times 10^{-4}$ au Å$^{-1}$; SCF = $10^{-8}$), and $[Pu(N(TePH_2)_2)_3]$ (maximum force = $8 \times 10^{-4}$ au Å$^{-1}$; SCF = $10^{-5}$). A natural charge and population analysis[40−46] was carried out on all G03 optimized structures. Little spin contamination was found for the quadruplet U(III) complexes, as evidenced by the fact that the values of $\langle S^2 \rangle$ were close to 3.75

(28) *APEX II 1.08*; Bruker AXS: Madison, WI, 2004.
(29) *SAINT+ 7.06*; Bruker AXS: Madison, WI, 2003.
(30) Sheldrick, G. *SADABS 2.03*; University of Göttingen: Göttingen, Germany, 2001.
(31) *SHELXTL 5.10*; Bruker AXS: Madison, WI, 1997.
(32) Frisch, M. J.; et al. *Gaussian 03*, revision D.01; Gaussian: Wallingford, CT, 2004.
(33) (a) ADF, SCM, Theoretical Chemistry, Vrije Universiteit, Amsterdam, The Netherlands (http://www.scm.com). (b) Fonseca Guerra, C.; Snijders, J. G.; te Velde, G.; Baerends, E. J. *Theor. Chem. Acc.* **1998**, *99*, 391. (c) te Velde, G.; Bickelhaupt, F. M.; Baerends, E. J.; Fonseca Guerra, C.; van Gisbergen, S. J. A.; Snijders, J. G.; Ziegler, T., J. *Comput. Chem.* **2001**, *22*, 931.
(34) Perdew, J. P.; Burke, K.; Ernzerhof, M. *Phys. Rev. Lett.* **1996**, *77*, 3865.
(35) Perdew, J. P.; Burke, K.; Ernzerhof, M. *Phys. Rev. Lett.* **1997**, *78*, 1396.
(36) Cao, X.; Dolg, M. *J. Mol. Struct. (THEOCHEM)* **2004**, *673*, 203.
(37) Bergner, A.; Dolg, M.; Küchle, W.; Stoll, H.; Preu$\beta$, H. *Mol. Phys.* **1993**, *80*, 1431.
(38) Hehre, W. J.; Stewart, R. F.; Pople, J. A. *J. Chem. Phys.* **1969**, *51*, 2657.
(39) Collins, J. B.; Schleyer, P. v. R.; Binkley, J. S.; Pople, J. A. *J. Chem. Phys.* **1976**, *64*, 5142.
(40) Carpenter, J. E.; Weinhold, F. *J. Mol. Struct. (THEOCHEM)* **1988**, *169*, 41.
(41) Carpenter, J. E. Ph.D. Thesis, University of Wisconsin: Madison, WI, 1987.
(42) Foster, J. P.; Weinhold, F. *J. Am. Chem. Soc.* **1980**, *102*, 7211.
(43) Reed, A. E.; Weinhold, F. *J. Chem. Phys.* **1983**, *78*, 4066.
(44) Reed, A. E.; Weinstock, R. B.; Weinhold, F. *J. Chem. Phys.* **1985**, *83*, 735.
(45) Reed, A. E.; Curtiss, L. A.; Weinhold, F. *Chem. Rev.* **1988**, *88*, 899.

**Table 1.** Selected Crystallographic Data for $M[N(EPPh_2)_2]_3$·solvate[a] and $M[N(EPiPr_2)_2]_3$ Complexes[b]

(a) $M[N(EPPh_2)_2]_3$ Complexes

| | compd **1** [25] | compd **2** | compd **3** | compd **4** | compd **5** [25] | compd **6** | compd **7** | compd **8** |
|---|---|---|---|---|---|---|---|---|
| empirical formula | $C_{79}H_{68}N_3P_6S_6U$ | $C_{79}H_{68}LaN_3P_6S_6$ | $C_{79}H_{68}N_3P_6PuS_6$ | $C_{79}H_{68}CeN_3P_6S_6$ | $C_{78}H_{60}D_6N_3P_6Se_6U$ | $C_{79}H_{68}LaN_3P_6Se_6$ | $C_{79}H_{68}N_3P_6PuSe_6$ | $C_{79}H_{68}CeN_3P_6Se_6$ |
| fw | 1675.63 | 1576.57 | 1676.66 | 1577.78 | 1948.99 | 1857.93 | 1958.03 | 1859.15 |
| space group | $R\bar{3}c$ | $R\bar{3}c$ | $R\bar{3}c$ | $R\bar{3}c$ | $R\bar{3}c$ | $R\bar{3}c$ | $R\bar{3}c$ | $R\bar{3}c$ |
| *a* (Å) | 15.0066(9) | 15.0368(7) | 15.0053(4) | 15.0131(3) | 15.1699(10) | 15.1824(5) | 15.1505(4) | 15.1571(3) |
| *b* (Å) | 15.0066(9) | 15.0368(7) | 15.0053(4) | 15.0131(3) | 15.1699(10) | 15.1824(5) | 15.1505(4) | 15.1571(3) |
| *c* (Å) | 56.107(4) | 56.186(5) | 56.133(4) | 56.130(2) | 56.846(7) | 57.129(4) | 56.984(3) | 57.057(3) |
| α (deg) | 90.00 | 90.00 | 90.00 | 90.00 | 90.00 | 90.00 | 90.00 | 90.00 |
| *β* (deg) | 90.00 | 90.00 | 90.00 | 90.00 | 90.00 | 90.00 | 90.00 | 90.00 |
| *γ* (deg) | 120.00 | 120.00 | 120.00 | 120.00 | 120.00 | 120.00 | 120.00 | 120.00 |
| *V* (Å$^3$) | 10942 4(12) | 11002.0(12) | 10945.5(8) | 10956.4(5) | 11329.1(18) | 11404.2(10) | 11327.6(7) | 11352.0(6) |
| Z | 6 | 6 | 6 | 6 | 6 | 6 | 6 | 6 |
| R1 | 0.0234 | 0.0305 | 0.0255 | 0.0338 | 0.0270 | 0.0257 | 0.0206 | 0.0232 |
| wR2 | 0.0564 | 0.0679 | 0.0618 | 0.1039 | 0.0678 | 0.0497 | 0.0536 | 0.0480 |

(b) $M[N(EPiPr_2)_2]_3$ Complexes

| | compd **9** | compd **10** | compd **11** | compd **12** | compd **13** | compd **14** | compd **15** | compd **16** [24] | compd **17** [24] | compd **18** | compd **19** |
|---|---|---|---|---|---|---|---|---|---|---|---|
| empirical formula | $C_{36}H_{84}N_3P_6S_6U$ | $C_{36}H_{84}LaN_3P_6S_6$ | $C_{36}H_{84}N_3P_6PuS_6$ | $C_{36}H_{84}CeN_3P_6S_6$ | $C_{36}H_{84}N_3P_6Se_6U$ | $C_{36}H_{84}LaN_3P_6Se_6$ | $C_{36}H_{84}N_3P_6PuSe_6$ | $C_{36}H_{84}N_3P_6Te_6U$ | $C_{36}H_{84}LaN_3P_6Te_6$ | $C_{36}H_{84}N_3P_6PuTe_6$ | $C_{36}H_{84}CeN_3P_6Te_6$ |
| fw | 1175.27 | 1076.15 | 1176.32 | 1077.36 | 1456.67 | 1357.55 | 1457.69 | 1748.51 | 1649.39 | 1749.53 | 1650.60 |
| space group | $P\bar{1}$ | $P\bar{1}$ | $P\bar{1}$ | $P\bar{1}$ | *C*2/*c* | $P2_1/c$ | *C*2/*c* | $P2_1/c$ | $P2_1/c$ | $P2_1/c$ | $P2_1/c$ |
| *a* (Å) | 12.974(3) | 13.0101(11) | 12.941(4) | 13.042(3) | 23.649(2) | 22.156(4) | 23.531(8) | 22.3600(18) | 22.456(6) | 22.348(2) | 22.235(2) |
| *b* (Å) | 13.333(3) | 12.3384(11) | 13.320(4) | 13.340(3) | 13.1855(12) | 13.517(2) | 13.118(5) | 13.7678(11) | 13.866(4) | 13.7485(15) | 13.8343(14) |
| *c* (Å) | 18.787(4) | 18.7969(15) | 18.779(5) | 18.965(4) | 19.6924(18) | 20.325(4) | 19.625(7) | 20.6919(17) | 20.828(5) | 20.723(2) | 20.843(2) |
| α (deg) | 91.189(4) | 91.1880(10) | 90.930(4) | 90.672(3) | 90.00 | 90.00 | 90.00 | 90.00 | 90.00 | 90.00 | 90.00 |
| *β* (deg) | 108.914(4) | 108.7370(10) | 109.056(3) | 109.289(3) | 115.2850(10) | 114.051(3) | 115.520(6) | 113.405(2) | 113.295(3) | 113.6330(10) | 113.5540(10) |
| *γ* (deg) | 117.146(4) | 117.2740(10) | 117.154(3) | 117.232(2) | 90.00 | 90.00 | 90.00 | 90.00 | 90.00 | 90.00 | 90.00 |
| *V* (Å$^3$) | 2680.5(11) | 2690.4(4) | 2669.3(13) | 2716.6(9) | 5552.3(9) | 5558.4(17) | 5467(3) | 5845.8(8) | 5957(3) | 5833.0(11) | 5877.1(11) |
| Z | 2 | 2 | 2 | 2 | 4 | 4 | 4 | 4 | 4 | 4 | 4 |
| R1 | 0.0609 | 0.0412 | 0.0413 | 0.0383 | 0.0318 | 0.0457 | 0.0868 | 0.0383 | 0.0544 | 0.0484 | 0.0395 |
| wR2 | 0.1447 | 0.0924 | 0.0731 | 0.0684 | 0.0841 | 0.0932 | 0.1558 | 0.0643 | 0.1285 | 0.0882 | 0.0568 |

[a] Solvate = toluene except for **5** where it is $C_6D_6$. $T$ = 141(2) K for all compounds except for **5** where $T$ = 203(2) K. [b] $T$ = 141(2) K for all compounds except for **12** where $T$ = 203(2) K.

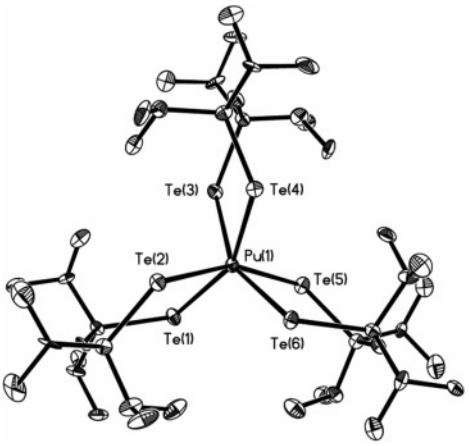


**Figure 2.** Thermal ellipsoid plot (at the 50% probability level) of the structure of $Pu[N(TeP{i}Pr_2)_2]_3$ (**18**), with the H atoms omitted for clarity. The complexes **9**−**17** and **19** have identical connectivity.

in all cases, with 3.770 for $[U(N(TePH_2)_2)_3]$ being the largest deviation from the ideal. Similar results were found for the Ce systems, with 0.757 being the largest deviation from the ideal 0.75 (for the Te complex). Spin contamination in the Pu complexes is more significant than in the U and Ce complexes; however the largest $\langle S^2 \rangle$ calculated was 8.865 for $[Pu(N(TePH_2)_2)_3]$, not a significant deviation from the ideal 8.75.

**2.3.2 ADF.** Single-point calculations on optimized G03 structures were carried out in ADF. As with G03 the PBE functional was used. TZP zero-order regular approximation (ZORA) basis sets were used for each of the f elements together with DZP ZORA basis sets for O, S, Se, P, and N; DZ was used for H. ADF does not have a DZP basis set for Te, so TZP polarization functions were added to the DZ basis. The frozen-core approximation was used. A 5d core was used for each actinide; 4d for the lanthanides and Te, 3d for Se, 2p for S, P, and 1s for O, N. Mulliken overlap population analyses[47,48] were carried out.

**2.3.3. Ligand Models and Point Group Symmetry.** As noted in the Introduction, we have thus far focused the computational studies on the experimentally characterized $M[N(EP{i}Pr_2)_2]_3$ systems. However the use of the *i*Pr groups in the calculations is extremely time-consuming, so, to cut computational cost, we tested two approximations by substituting *i*Pr for H or Me. Since we sought to model the R = *i*Pr complexes, only six-coordinate complexes with local energy minima were considered, and we did not examine the possibility that a global energy minimum could result in a nine-coordinate complex with both E and N coordination to the metal. Extensive tests (data not shown here) on the energies, bond lengths, and charges of these complexes revealed that the choice of R group does not affect the metal−chalcogen bond lengths or charges to any significant extent. We also tested the validity of idealizing the geometries to the $D_3$ symmetry group (with its favorable consequences for electronic structure analysis), and again concluded that this has little impact upon the quality of the results. Thus the present paper focuses on studies in the $D_3$ point group.

## 3. Results

**3.1. Syntheses, Structure, and Characterization of $M[N(EPPh_2)_2]_3$ Complexes.** Treatment of $M[N(SiMe_3)_2]_3$ (M = U, Pu, La, or Ce) with 3 equiv of $NH(EPPh_2)_2$ (E = S, Se) in THF/toluene results in ligand deprotonation and coordination to the metal ion, to afford the neutral $M[N(EPPh_2)_2]_3$ (**1**−**8**) complexes (eq 1).

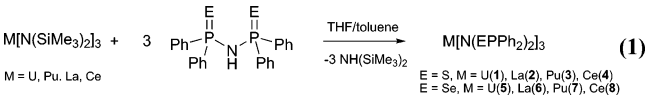

**(1)**

The molecular structures of **1**−**8** (Figure 1, Table 1a) consist of nine-coordinate metal centers and anions that are tridentate through both chalcogen atoms and the nitrogen atom. The geometry about the metal center is best described as distorted tricapped trigonal prismatic. Although ionic radii are available for nine-coordinate La(III) and Ce(III), none are available for nine-coordinate U(III) or Pu(III).[49] The ionic radii for six-coordinate U(III) and La(III) are 1.025 and 1.032 Å, respectively, whereas those for six-coordinate Pu(III) and Ce(III) are 1.00 and 1.01 Å, respectively. Because we wish to compare bond distances involving 5f and 4f trivalent cations of similar size, we chose the U(III)/La(III) and Pu(III)/Ce(III) pairs (Table 2). Judging from the limited data available,[49] we believe that the difference in radii for nine coordination within these pairs remains essentially the same as it is for six coordination. As an example, the ionic radius of Ce(IV) increases by 0.27 Å on going from six coordination to twelve coordination; the corresponding increase in the radius of U(IV) is 0.28 Å. The salient bond distances for comparison are summarized in Table 2. The U−S distance is 2.9956(5) Å in **1** and is shorter than the La−S distance of 3.0214(11) in **2** by 0.026(1) Å, a significantly larger difference than the difference in ionic radii between U(III) and La(III) of 0.007 Å. The corresponding difference in bond lengths is 0.0360(5) Å between a U−Se distance of 3.0869(4) Å in **5** and a La−Se distance of 3.1229(3) Å in **6**. Whereas **5** is a deuterobenzene solvate, **6** is a toluene solvate. We assume that the difference in bond lengths is not affected by the difference in solvents.

**Table 2.** Selected Bond Distances (Å) for $M[N(EPPh_2)_2]_3$ Complexes

| compd | bond | distance | bond | distance | difference[a] |
|---|---|---|---|---|---|
| $U[N(SPPh_2)_2]_3$ (**1**) | U−N | 2.632(2) | U−S | 2.9956(5) | |
| $La[N(SPPh_2)_2]_3$ (**2**) | La−N | 2.652(4) | La−S | 3.0214(11) | 0.026(1) |
| $Pu[N(SPPh_2)_2]_3$ (**3**) | Pu−N | 2.612(3) | Pu−S | 2.9782(6) | |
| $Ce[N(SPPh_2)_2]_3$ (**4**) | Ce−N | 2.637(3) | Ce−S | 3.0052(6) | 0.0270(8) |
| $U[N(SePPh_2)_2]_3$ (**5**) | U−N | 2.701(3) | U−Se | 3.0869(4) | |
| $La[N(SePPh_2)_2]_3$ (**6**) | La−N | 2.706(3) | La−Se | 3.1229(3) | 0.0360(5) |
| $Pu[N(SePPh_2)_2]_3$ (**7**) | Pu−N | 2.668(2) | Pu−Se | 3.0710(2) | |
| $Ce[N(SePPh_2)_2]_3$ (**8**) | Ce−N | 2.691(3) | Ce−Se | 3.1013(3) | 0.0303(4) |

[a] Difference is between An−E and Ln−E bond lengths.

The comparison of bond lengths between the Pu(III) and Ce(III) complexes also reveals significantly shorter actinide−chalcogen bonds relative to lanthanide−chalcogen bonds. The Pu−S bond length in **3** is 2.9782(6) Å compared to 3.0052(6) Å for Ce−S in **4**, a difference of 0.0270(8) Å. This difference is 0.0303(4) Å in the Se analogue, with a Pu−Se distance in **7** of 3.0710(2) Å and a Ce−Se distance in **8** of 3.1013(3) Å. The Se−M−Se angles are slightly larger

(46) Weinhold, F.; Carpenter, J. E. In *The Structure of Small Molecules and Ions*; Naaman, R., Vager, Z., Eds.; Plenum Press: New York, 1988; p 227.
(47) Politzer, P.; Mulliken, R. S. *J. Chem. Phys.* **1971**, *55*, 5135.
(48) Grier, D. L.; Streitwieser, A., Jr. *J. Am. Chem. Soc.* **1982**, *104*, 3556.
(49) Shannon, R. D. *Acta Crystallogr.* **1976**, *A32*, 751.

**Table 3.** $^{31}$P NMR Shifts (ppm) for M[N(EPR$_2$)$_2$]$_3$ Complexes

| compd | $^{31}$P NMR shift (ppm) | compd | $^{31}$P NMR shift (ppm) |
|---|---|---|---|
| U[N(SePPh$_2$)$_2$]$_3$ (**5**) | −722.6 | Ce[N(TeP*i*Pr$_2$)$_2$]$_3$ (**19**) | −10.0 |
| U[N(TeP*i*Pr$_2$)$_2$]$_3$ (**16**) | −696.7 | Ce[N(SePPh$_2$)$_2$]$_3$ (**8**) | −8.3 |
| U[N(SPPh$_2$)$_2$]$_3$ (**1**) | −680.6 | Pu[N(SP*i*Pr$_2$)$_2$]$_3$ (**11**) | −1.4 |
| U[N(SeP*i*Pr$_2$)$_2$]$_3$ (**13**) | −573.9 | Ce[N(SPPh$_2$)$_2$]$_3$ (**4**) | 4.9 |
| U[N(SP*i*Pr$_2$)$_2$]$_3$ (**9**) | −525.1 | La[N(TeP*i*Pr$_2$)$_2$]$_3$ (**17**) | 29.5 |
| Pu[N(TeP*i*Pr$_2$)$_2$]$_3$ (**18**) | −62.2 | La[N(SePPh$_2$)$_2$]$_3$ (**6**) | 33.6 |
| Pu[N(SePPh$_2$)$_2$]$_3$ (**7**) | −59.2 | La[N(SPPh$_2$)$_2$]$_3$ (**2**) | 42.6 |
| Pu[N(SPPh$_2$)$_2$]$_3$ (**3**) | −47.1 | La[N(SeP*i*Pr$_2$)$_2$]$_3$ (**14**) | 56.8 |
| Pu[N(SeP*i*Pr$_2$)$_2$]$_3$ (**15**) | −20.1 | La[N(SP*i*Pr$_2$)$_2$]$_3$ (**10**) | 64.3 |

than the S−M−S angles, presumably owing to the larger size of Se compared to S. The [EPNPE] linkage has minor deviations from planarity with the angle between the PE$_2$ and ME$_2$ planes ranging from 5.2 to 6.0 °.

Although not the direct focus of this study, in the M[N(EPPh$_2$)$_2$]$_3$ complexes **1**−**8**, M is coordinated to both E and to N. Nitrogen is a softer donor atom than oxygen, and it is of interest to also compare the An−N distances to the Ln−N distances. The M−N distances in **1**−**8** are statistically different in three of the four comparisons. The U−N distance in **1** is shorter than the La−N distance in **2** by 0.020(4) Å, Pu−N in **3** shorter than Ce−N in **4** by 0.025(4) Å, U−N in **5** shorter than La−N in **6** by 0.005(4) Å, and Pu−N in **7** shorter than Ce−N in **8** by 0.023(4) Å.

La(III) is diamagnetic (4f$^0$), and complexes **2** and **6** display resonances at 42.6 and 33.6 ppm, respectively, in the $^{31}$P NMR spectra (Table 3). The other complexes (**1**, **3**−**5**, **7**, **8**) all display paramagentically shifted resonances (Ce(III), 4f$^1$; U(III), 5f$^3$; Pu(III), 5f$^5$), with the U(III) complexes displaying the largest downfield chemical shifts, with a resonance at −722.6 ppm for U[N(SePPh$_2$)$_2$]$_3$ (**5**). The resonances for the Pu(III) and Ce(III) complexes are shifted to a much lesser extent. The UV/vis/near-IR spectra of the Pu and U complexes have absorbances resulting from Laporte forbidden 5f−5f transitions and allowed 5f−6d transitions, with multiple absorption bands in the 500−1300 nm region. There are also intense charge-transfer bands below 500 nm.

We were unable to isolate the analogous Te donor complexes. Treatment of UI$_3$(THF)$_4$ with [Na(tmeda)-{N(TePPh$_2$)$_2$}] resulted in Te$^{II}$[N(TePPh$_2$)$_2$]$_2$ as the only tractable product and a gray powder, which was most likely elemental Te. However, as we describe in the next section, replacement of the phenyl rings on the ligands with *i*Pr groups allows access to the Te donor complexes.

**3.2. Syntheses, Structure, and Characterization of M[N(EP*i*Pr$_2$)$_2$]$_3$ Complexes.** Treatment of M[N(SiMe$_3$)$_2$]$_3$ (M = U, Pu, La, or Ce) with 3 equiv of NH(EP*i*Pr$_2$)$_2$ (E = S, Se) in THF or treatment of MI$_3$(py)$_4$ (sol = py, M = U, Pu; sol = THF, M = La, Ce) with 3 equiv of [Na(tmeda)-{N(TeP*i*Pr$_2$)$_2$}] in Et$_2$O yields the neutral M[N(EP*i*Pr$_2$)$_2$]$_3$ (**9**−**19**) complexes (eqs 2 and 3). We were unable to isolate the Ce[N(SeP*i*Pr$_2$)$_2$]$_3$ complex. We could not isolate a bulk quantity of Ce[N(SP*i*Pr$_2$)$_2$]$_3$ to allow spectroscopic characterization, so only the crystal structure was determined. The molecular crystal structures of **9**−**19** (Figure 2, Table 1b) consist of six-coordinate metal centers and anions that are bidentate through both chalcogen atoms. The N atoms of the ligands do not coordinate. The geometry about the metal

**Table 4.** Selected Bond Distances (Å) for M[N(EP*i*Pr$_2$)$_2$]$_3$ Complexes[a]

| compd | bond | av distance | difference |
|---|---|---|---|
| U[N(SP*i*Pr$_2$)$_2$]$_3$ (**9**) | U−S | 2.854(7) | |
| La[N(SP*i*Pr$_2$)$_2$]$_3$ (**10**) | La−S | 2.892(1) | 0.038(7) |
| Pu[N(SP*i*Pr$_2$)$_2$]$_3$ (**11**) | Pu−S | 2.819(3) | |
| Ce[N(SP*i*Pr$_2$)$_2$]$_3$ (**12**) | Ce−S | 2.864(2) | 0.045(4) |
| U[N(SeP*i*Pr$_2$)$_2$]$_3$ (**13**) | U−Se | 2.964(7) | |
| La[N(SeP*i*Pr$_2$)$_2$]$_3$ (**14**) | La−Se | 3.019(3) | 0.055(8) |
| Pu[N(SeP*i*Pr$_2$)$_2$]$_3$ (**15**) | Pu−Se | 2.917(4) | |
| U[N(TeP*i*Pr$_2$)$_2$]$_3$ (**16**) | U−Te | 3.164(2) | |
| La[N(TeP*i*Pr$_2$)$_2$]$_3$ (**17**) | La−Te | 3.224(3) | 0.060(4) |
| Pu[N(TeP*i*Pr$_2$)$_2$]$_3$ (**18**) | Pu−Te | 3.123(3) | |
| Ce[N(TeP*i*Pr$_2$)$_2$]$_3$ (**19**) | Ce−Te | 3.182(1) | 0.059(3) |

[a] Esd's associated with the average distances were determined by summing the squares of the esd associated with each of the six independent M−E bonds and taking the square root of that value.

center is best described as distorted trigonal prismatic. Selected crystallographic data are provided in Table 1b, and the salient bond distances are summarized in Table 4. For comparative purposes we have chosen to use average M−E bond distances to identify differences in bonding. In this respect, the following caveats are noted. Compounds **9**−**12** crystallize in the space group $P\bar{1}$, and compounds **14** and **16**−**19** crystallize in the space group $P2_1/c$. All of these complexes have three long and three short M−E bonds (one long and one short bond per ligand). Compounds **13** and **15** both crystallize in the space group $C2/c$, and because of symmetry one of the ligands in these complexes has two identical M−E lengths, whereas the other two ligands each have one short and one long M−E bond. All of the U/La and Pu/Ce comparisons are between isostructural compounds with the exception of **13** (U[N(SeP*i*Pr$_2$)$_2$]$_3$ in space group $C2/c$) and **14** (La[N(SeP*i*Pr$_2$)$_2$]$_3$ in space group $P2_1/c$). In comparing the bond distances between **13** and **14** the fact that they are not in the same space group is ignored. Compound **15** (Pu[N(SeP*i*Pr$_2$)$_2$]$_3$) does not have a lanthanide counterpart for comparison because we were unable to crystallize Ce[N(SeP*i*Pr$_2$)$_2$]$_3$.

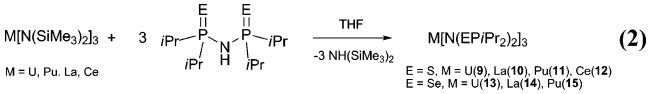


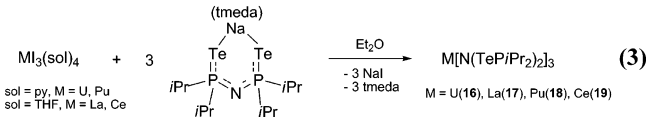


In the R = *i*Pr series of compounds the crystallographically independent M−E distances frequently differ significantly. We have chosen to average M−E distances for a given compound. The resultant differences among average U−E

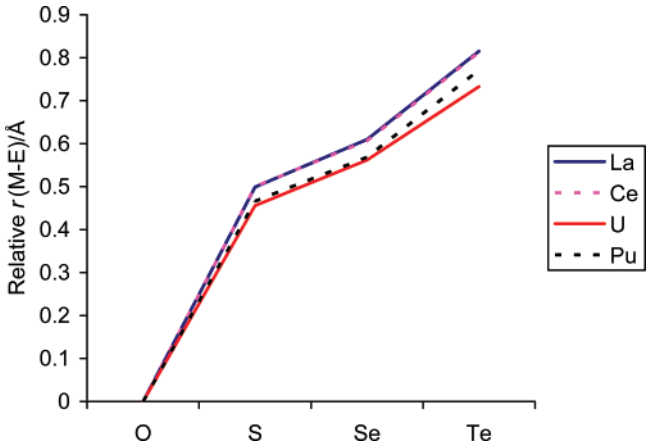


**Figure 3.** Relative calculated $r$(M−E) for M[N(EPH$_2$)$_2$]$_3$ (M = La, U, Pu, Ce; E = O, S, Se, Te) at the optimized geometries. $r$(M−O) has been set to zero for each metal.

vs La−E and Pu−E vs Ce−E distances are necessarily less accurate than for the R = Ph series of compounds (which contain only one independent M−E distance). Nevertheless, the resultant differences for the R = *i*Pr series of compounds (Table 4) show the same trends as do those for the R = Ph series of compounds (Table 2). Specifically, the average U−S distance is 2.854(7) Å in **9** and is shorter than the average La−S distance of 2.892(1) Å in **10** by 0.038(7) Å. The average U−Se distance of 2.964(7) Å in **13** is shorter than the average La−Se of 3.019(3) Å in **14** by 0.055(8) Å. The average U−Te distance is 3.164(2) Å in **16** and is shorter than the average La−Te of 3.224(3) Å in **17** by 0.060(4) Å. Moving along the f-element series, we observe significant bond length differences between the Pu(III) and Ce(III) complexes. The average Pu−S distance of 2.819(3) Å in **11** is shorter than the average Ce−S distance of 2.864(2) in **12** by 0.045(4) Å. The average Pu−Te distance of 3.123(3) Å in **18** is shorter than the average Ce−Te distance of 3.182(1) Å in **19** by 0.059(3) Å.

The E−M−E bite angles are smaller than the angles in the tridentate R−Ph complexes, reflecting the absence of N coordination. As was observed in the R = Ph complexes, the E−M−E bite angles increase as the chalcogen group is descended from S to Se to Te and the size of the donor atom increases. The ligands in the R = *i*Pr complexes, **9**−**19**, are twisted to a greater extent than are those in the R = Ph complexes. This is likely a result of the greater steric hindrance of the *i*Pr groups relative to the phenyl rings, which results in the inability of the N atoms to coordinate to the metal. The angles between the ME$_2$ and MP$_2$ planes range from 21.5 to 24.5°, compared to only 5.2 to 6.0° in the R = Ph tridentate complexes.

In the $^{31}$P NMR spectra (Table 3), the diamagnetic La(III) (4f$^0$) complexes **10**, **14**, and **17** display resonances at 64.3, 56.8, and 29.5 ppm, respectively. The U(III), Pu(III) and Ce(III) complexes all display paramagnetic shifts, with the largest downfield shift observed for U[N(TeP*i*Pr$_2$)$_2$]$_3$ (**16**) at −696.7 ppm. The $^{31}$P NMR spectra also have resonances of small intensity at values for the free ligand suggesting that in solution there is some dissociation or decomposition of the complexes. This is supported by the $^1$H NMR spectra of the diamagnetic La(III) complexes **10** and **14**, which display resonances for the free ligand in addition to the metal complexes. The UV/vis/near-IR spectra of the Pu and U complexes have absorbances resulting from Laporte forbidden 5f−5f transitions and allowed 5f−6d transitions, with multiple absorption bands in the 500−1300 nm region. There are also intense charge-transfer bands below 500 nm.

**Table 5.** Selected Bond Distances (Å) for the Model (Calculated) M[N(EPH$_2$)$_2$]$_3$ Complexes

| compd | bond | av distance | difference |
|---|---|---|---|
| U[N(OPH$_2$)$_2$]$_3$ | U−O | 2.393 | |
| La[N(OPH$_2$)$_2$]$_3$ | La−O | 2.417 | 0.024 |
| Pu[N(OPH$_2$)$_2$]$_3$ | Pu−O | 2.364 | |
| Ce[N(OPH$_2$)$_2$]$_3$ | Ce−O | 2.390 | 0.026 |
| U[N(SPH$_2$)$_2$]$_3$ | U−S | 2.849 | |
| La[N(SPH$_2$)$_2$]$_3$ | La−S | 2.916 | 0.067 |
| Pu[N(SPH$_2$)$_2$]$_3$ | Pu−S | 2.830 | |
| Ce[N(SPH$_2$)$_2$]$_3$ | Ce−S | 2.890 | 0.060 |
| U[N(SePH$_2$)$_2$]$_3$ | U−Se | 2.955 | |
| La[N(SePH$_2$)$_2$]$_3$ | La−Se | 3.027 | 0.072 |
| Pu[N(SePH$_2$)$_2$]$_3$ | Pu−Se | 2.932 | |
| Ce[N(SePH$_2$)$_2$]$_3$ | Ce−Se | 2.996 | 0.064 |
| U[N(TePH$_2$)$_2$]$_3$ | U−Te | 3.126 | |
| La[N(TePH$_2$)$_2$]$_3$ | La−Te | 3.232 | 0.106 |
| Pu[N(TePH$_2$)$_2$]$_3$ | Pu−Te | 3.135 | |
| Ce[N(TePH$_2$)$_2$]$_3$ | Ce−Te | 3.202 | 0.067 |

**3.3. Density Functional Theory Calculations. 3.3.1. Structural Data.** The calculated M−E bond distances, $r$(M−E), for M[N(EPH$_2$)$_2$]$_3$ (M = La, U, Pu, Ce; E = O, S, Se, Te) are given in Table 5. The calculated $r$(M−E) agree very well with experiment in all cases for which data are available; the maximum discrepancy between theory and experiment is ca. 0.04 Å, and the mean absolute difference is less than 0.02 Å in all cases. As the chalcogen is changed from O to Te, $r$(M−E) lengthens significantly, the increase being largest between O and S, followed by a smaller increase from S through Se to Te. $r$(M−O) is similar for all four metals, and the difference between analogous $r$(Ln−E) and $r$(An−E) pairs increases down group 16. Figure 3 emphasizes this point by normalizing $r$(M−O) to zero for each of the metals. It can clearly be seen that whereas $r$(U−E) increases as the chalcogen becomes heavier, $r$(Pu−E) increases slightly more steeply and $r$(Ln−E) increases considerably more steeply. Thus, while $r$(La−O) is ca. 0.02 Å longer than $r$(U−O), $r$(La−Te) is ca. 0.11 Å longer than $r$(U−Te). A similar, though less dramatic, pattern is observed for Ce and Pu; $r$(Ce−O) is ca. 0.03 Å longer than $r$(Pu−O) and $r$(Ce−Te) is ca. 0.07 Å longer than $r$(Pu−Te). These calculated structural data suggest that U−E and Pu−E bonding for the heavier chalcogens is indeed somewhat different from that in the analogous Ln complexes. We also note that while the general trend of differences between An−E and Ln−E bond lengths from the structural data are replicated computationally, the calculated differences are slightly larger than the experimentally observed differences. In addition the DFT studies predict a smaller difference between Pu−E and Ce−E bond lengths compared to those between U−E and La−E, a phenomenon, which within experimental errors, was not observed from the single-crystal X-ray structural data.

**3.3.2. Natural Charges and Populations.** The natural charges for selected atoms are presented in the Supporting

Information. It is immediately apparent that the charges on the I N, and P atoms are rather similar for all four metals for a given chalcogen. The principal difference between the complexes comes in the metal charges, which for all E decrease in the order $q_{La} > q_{Ce} > q_{Pu} > q_U$. It is noticeable that the difference in $q_M$ for analogous Ln/An pairs is significantly smaller for Ce/Pu than for La/U. For the latter, $q_{La}$ is ca. 13% larger than $q_U$ in the O system, a difference which increases to 25% for S and Se before reducing to ca. 20% for Te. By contrast, the difference in the Ce/Pu compounds is ca. 6% for O, rising to ca. 10% for the heavier chalcogens. This suggests that while the metal−chalcogen bond in both the La and Ce compounds is more polar than in their actinide equivalents, this difference in ionicity is larger for the La/U pair than for the Ce/Pu pair. Further evidence for this comes from examination of the charge differences between M and E as a function of both metal and chalcogen. For La, there is a ca. 36% reduction in $q_{La} - q_{E(La)}$ as E is altered from O to Te. For the other metals, the corresponding values are ca. 38% for Ce, ca. 40% for Pu, and ca. 41% for U. Thus, the decrease in ionicity down group 16 is largest for the U compounds and smallest for the La compounds, and hence the natural charges reinforce the conclusions from the calculated and experimental geometries that the bonding in the actinide systems, particularly the U complexes, is somewhat different from that in the lanthanides.

The natural atomic orbital populations for the metals are presented in the Supporting Information. The values given have been obtained by subtracting the formal values from the calculated ones; i.e., they show the enhancement of the populations above the formal. In each case the latter is 2 for the s orbitals, 6 for the p, and 0 for the d. The formal f populations are 0 for La(III), 1 for Ce(III), 3 for U(III), and 5 for Pu(III). It is immediately apparent that the $(n - 1)$p populations are essentially unaltered from their formal values in all cases. By contrast, there are increases of the other orbital populations above their formal values, which may be taken as evidence of the involvement of these orbitals in covalent bonding with the ligands. For all four metals, the s population increases as group 16 is descended, and the extent of this increase is broadly similar in all cases. The d populations also increase down group 16 by an amount that is generally slightly more significant than for the s. By contrast, the f populations do not change very much as group 16 is descended. There is a slight reduction from O to Te in the La and Ce f populations, while those for Pu are very similar in all four complexes. For U, there is greater variability, with no clear pattern down group 16.

We conclude that the natural populations support the charges in finding greater covalency as group 16 is descended for all four metals. This increase in covalency arises from increases in metal d and, to a slightly lesser extent, s populations from O to Te. By contrast, there is no such increase in metal f population down group 16, although it is noticeable that the f populations for the actinides are larger than for the lanthanides. This suggests that while increases in covalency down group 16 are a function of the metal s and d orbitals, the actinide complexes are more covalent than their lanthanide counterparts on account of the greater involvement of the 5f orbitals over the 4f orbitals.

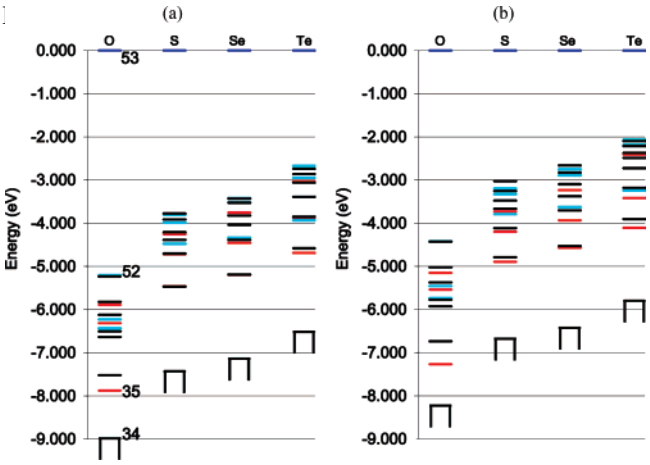


**Figure 4.** Molecular orbital energy level diagrams for $M[N(EPH_2)_2]_3$ (M = La (a) and U (b); E = O, S, Se, Te), calculated in the $D_3$ point group. The energy of the lowest unoccupied orbital of each of the La complexes (number 53, shown in dark blue) has been set to an energy of 0 eV, as has the energy of the most stable of the highest occupied (5f-based) orbitals of the U complexes (also shown in dark blue). The mean energies of the α- and $\beta$-spin components of each spatial MO are presented for the U compounds. For orbitals 35−52, red indicates $a_1$ symmetry MOs, turquoise $a_2$ MOs, and black e MOs.

**3.3.3. Mulliken Overlap Populations.** Calculated Mulliken overlap populations for the target complexes are presented in the Supporting Information. Two sets of data are provided for each metal. The first set is the overlap population between the metal atom and an individual chalcogen, while the second set is for the interaction of an $M^{3+}$ center with the trianionic ligand set. Mulliken overlap populations can be considered as the number of electrons covalently bonding between two atoms or groups of atoms. Both sets of data suggest enhanced covalency in the compounds of the heavier chalcogens for all four metals, in agreement with the conclusions from the natural charge and population analyses. Both the Ln−E and $Ln^{3+}-L_3^{3-}$ data for the two families of lanthanide compounds are very similar to one another. Comparison of La and Ce with U, however, reveals significantly larger overlap populations in the actinide systems, at least for E = S, Se, and Te, suggesting greater covalency in the U compounds. The Pu data generally lie between the Ln and U values, indicating that the bonding in the Pu complexes is intermediate in covalency between that in the compounds of the early 4f elements and U.

**3.3.4. Molecular Orbital Structure.** To test further the conclusions drawn from the natural and Mulliken analyses, we have probed the molecular orbital structure of the La and U complexes. MO energy level diagrams for $M[N(EPH_2)_2]_3$ (E = O, S, Se, Te) are given in Figure 4 for (a) M = La and (b) M = U. To allow the electronic structures to be better compared, the diagrams have been constructed by arbitrarily setting the energy of the lowest unoccupied orbital of each of the La complexes to an energy of 0 eV. This orbital (number 53) is predominantly (>95%) 4f in character in all four cases. For the U systems, the highest occupied orbitals contain the anticipated three 5f electrons, and the energy of

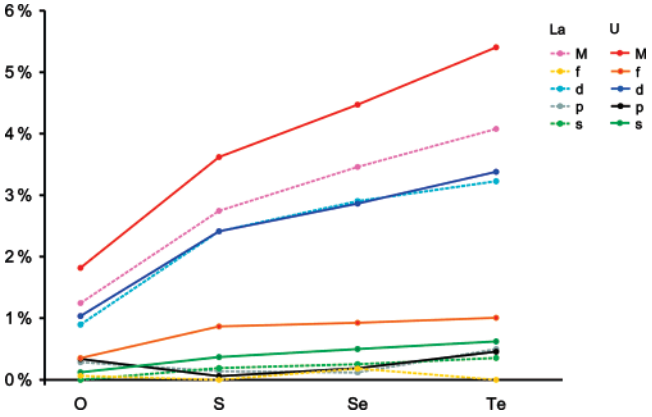


**Figure 5.** Average metal contributions to orbitals 35−52 (see Figure 4) for $M[N(EPH_2)_2]_3$ (M = La, U; E = O, S, Se, Te). For each metal, "M" indicates the average total metal contribution.

the most stable of these orbitals has been set to 0 eV in all cases. Given the open-shell nature of the U complexes, spin-unrestricted calculations were performed, yielding separate energies for the α- and *β*-spin components of each spatial orbital. Figure 4b presents the mean energies of the α- and *β*-spin components of each spatial MO.

In each $La[N(EPH_2)_2]_3$ (E = O, S, Se, Te) orbital 53 (the LUMO) is well-separated from the highest occupied levels by an energy gap that decreases from just over 5 eV in $La[N(OPH_2)_2]_3$ to just under 3 eV in $La[N(TePH_2)_2]_3$. Below the HOMO (orbital 52) there is a group of 18 orbitals, which spans a 2−3 eV energy range and which is well-separated from the next group of orbitals below (represented by the open-ended black boxes in Figure 4a). Figure 4b is very similar, although the group of orbitals from 35 to 52 lies ca. 0.5 eV closer to the U 5f-based levels on comparison of analogous La and U energy level diagrams.

The 18 orbitals from 35 to 52 are predominantly chalcogen *n*p-based in all cases. It is clear that their barycenter moves relative to the f-based orbitals as group 16 is descended; this is a result of the *n*p atomic orbital energies becoming less negative as the chalcogen becomes heavier. The reduced 52/53 gap in the U systems is most likely due to the U 5f orbitals being slightly more stable than the La 4f levels.

We have analyzed the composition of all 18 MOs for all eight $M[N(EPH_2)_2]_3$ (M = La, U; E = O, S, Se, Te), and in particular have focused on the contribution of the metals' valence atomic orbitals. These contributions have been averaged over all 18 orbitals, and the results are presented in Figure 5. It is clear that the average total metal contribution to these orbitals increases down group 16 for both La and U. Although the absolute values of these contributions may not seem large, it should be borne in mind that some of the MOs have no metal content at all, which obviously reduces the average contribution. Indeed, some of the 18 MOs have substantially more metal contribution than the average—well over 10% in some cases. See Figure 6 for a graphical representation of one of the calculated molecular orbitals.

It is noticeable that metal contributions in analogous La and U compounds are always larger in the actinide system. Figure 5 gives the average contribution of each of the metals' s-, p-, d-, and f-atomic orbitals. Clearly the largest contributor is in all cases the metal d orbitals, the trend in which mirrors the total metal contribution in increasing down group 16. It is interesting that although the total U orbital contribution is always larger than the total La orbital contribution, the metal d contributions to analogous 4f and 5f complexes are essentially the same. The orbital that is responsible for differentiating the average U total contribution from that of La is the f, which is more involved in the valence MOs of the actinide systems than the lanthanide (in which there is very little 4f contribution at all). Thus, the orbital composition data very much support our conclusions from the natural and Mulliken analyses in finding that (a) increases in covalency down group 16 for a given metal come primarily as a result of enhanced metal d involvement in the MOs and (b) the larger covalency in the actinide complexes is a function of greater 5f participation.

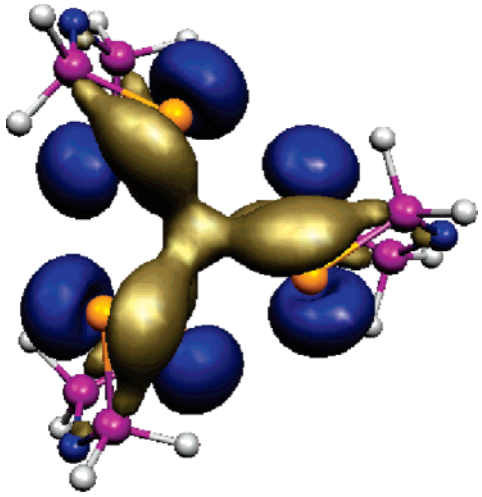

**Figure 6.** Representation of a calculated molecular orbital (orbital number 44 of $a_1$ symmetry) in the $U[N(SePH_2)_2]_3$ model complex.

## 4. Discussion

Differences in metal−ligand bond lengths can be used as a measure of relative covalency in the bonding between structurally similar 4f- and 5f-metal complexes, where the identity of the metals are different but they have near-identical ionic radii. This approach is based on the assumption that if the metal−ligand bonding were "completely ionic", then the bond distances would differ by the difference in the ionic radii of the metal ions. The ionic radius of U(III) most closely matches that of La(III), and the ionic radius of Pu(III) most closely matches that of Ce(III). Examination of the bond distances between U(III) and La(III) complexes and between Pu(III) and Ce(III) complexes reveals a trend that supports a modest increase in covalent contribution to the bonding in An(III) complexes compared to Ln(III) complexes. In the $M[N(EPPh_2)_2]_3$ complexes (**1**−**8**) the U−E distances are shorter than the La−E distances by a value significantly larger (ca. 0.03 Å) than just the difference between the ionic radii of U(III) and La(III) of 0.007 Å (Table 2). The difference is observed for both E = S and Se. Differences of values similar in magnitude are observed between the Pu−E and Ce−E bond lengths suggesting that

although Pu(III) is a more electropositive (harder) ion than U(III), the enhanced covalency relative to a 4f ion of the same size is still significant. In the $M[N(EPiPr_2)_2]_3$ complexes the ligands are bidentate, whereas in the $M[N(EPPh_2)_2]_3$ complexes the ligands are tridentate. The bidentate bonding mode is presumably a steric effect of the increased bulk of the *i*Pr groups relative to the Ph rings. As an interesting example of the importance of steric effects in these types of complexes, note that in $Y[N(SPPh_2)_2]_3$ the Y(III) is nine-coordinate, as it is in the present M(III) complexes, but in $Y[N(SePPh_2)_2]_3$ the Y(III) is only seven-coordinate.[50]

The M−E bond length differences in the $M[N(EPiPr_2)_2]_3$ complexes are larger (Table 4) than in the $M[N(EPPh_2)_2]_3$ complexes (Table 2), probably as a result of the nonbonding nature of the ligand N atom and concomitant reduction in the coordination number from nine to six. The $M[N(EPiPr_2)_2]_3$ complexes contain only M−E bonds and represent the "ideal" complexes for comparison because the possible effects from other donor atoms do not have to be considered. The largest difference in bond lengths is ca. 0.060 Å, observed for the softest donor atom in this study, between U−Te and La−Te in **16** and **17** and between Pu−Te and Ce−Te in **18** and **19**. Drawing these results together allows us to identify two general trends. First, the U−E bonds are all shorter than the corresponding La−E bonds, and the Pu−E bonds are all shorter than the corresponding Ce−E bonds. Second, as the chalcogen donor group is descended, the magnitude of the differences increases slightly, consistent with a greater covalent contribution to the bonding the softer the donor atom.

The calculated structural data, obtained on six-coordinate R = H model complexes, fully agree with experiment. Computationally when we alter the chalcogen donor all the way from O to Te, we find that for both the U(III)/La(III) and Pu(III)/Ce(III) pairs there is little difference in An−O/Ln−O distances, by contrast to significantly shorter An−E distances for the heavier chalcogens. Furthermore, analysis of the electronic structures of our target complexes at the calculated geometries yields convincing evidence that the M−E bonding in the actinide complexes of the heavier chalcogen donors is significantly more covalent than in the analogous lanthanide systems.

As mentioned in the Introduction, there have been several reported compounds that display actinide−ligand bonds that are ca. 0.03−0.1 Å shorter than the corresponding lanthanide−ligand bonds, consistent with the values observed in this study. However, these comparisons relate to U, an early actinide. Therefore, the comparison of Pu−E to Ce−E is of particular importance in addressing the issue of what the effect of the f-element contraction is upon bonding differences between 4f and 5f ions as the ions become smaller and have a greater positive charge density. Specifically, are there differences in bond lengths between Pu(III) and Ce(III) complexes, and are the magnitudes of those differences diminished compared to those observed between U(III) and La(III)? The answers to these questions are not only important for understanding the fundamental nature of bonding in the f elements but are also vital for underpinning Am/Cm/Eu separations in the nuclear industry.[1−16,20−23] The high specific activity and scarcity of suitable precursors have, to date, prevented a direct study of the nonaqueous coordination chemistry of Am(III) and Cm(III). However, here we have shown that upon moving two elements across the 5f series (from U to Pu), the structural data do not suggest a diminished degree of enhanced covalency. Analysis of the computational results, however, suggests that the covalency in the Pu complexes lies somewhere intermediate between that in the U and La/Ce complexes. It is clearly of importance that future work establishes the extent to which the enhanced An−E/Ln−E covalency still occurs by the time the minor actinides are reached. It may well be that a significant, but modest, enhanced covalency compared to a 4f ion of similar size is important in explaining the remarkable separation factors of soft donors for Am/Cm over Eu. The excellent agreement between theory and experiment in the U/La and Pu/Ce systems reported here leads us to propose that extension of our computational studies to the middle of both the 4f and 5f series will yield similarly reliable results. Such studies are underway. In this respect, given the practical difficulties of synthesizing and fully characterizing any but the most primitive of trans-plutonium coordination complexes, the establishment of a computational model that can be applied with confidence to Am(III) and Cm(III) complexes is of great importance. It must rely in no small part on experimental validation through studies of trivalent U, Np, and Pu systems, preferably of a nature similar to those in this present investigation, that allow systematic variations in structurally similar molecular compounds across the 4f and 5f series.

Although the primary focus of this research was a comparative study of An(III)/Ln(III) bonding, the syntheses of actinide complexes with chalcogen donors are of more general interest in advancing knowledge of the structure and bonding in molecular actinide complexes. There are very few reported molecular actinide complexes with the heavier chalcogens as donor atoms. There are only four examples of molecular crystal structures containing U−Se bonds[25,51−53] (only one U(III) complex) and three examples of a U−Te bond.[24,53] Complexes **7**, **15**, and **18** are the first examples of structural determinations of molecular Pu complexes with Se and Te donor atoms. Moreover, coordination chemistry studies of Pu are rare and, at the time of writing, there are only 29 entries for complexes containing Pu in the Cambridge Structural Database. About half of these are full molecular structural determinations, with the rest being limited to powder diffraction studies and cell constants. Examples of fully structurally characterized Pu complexes

(50) Pernin, C. G.; Ibers, J. A. *Inorg. Chem.* **2000**, *39*, 1222.
(51) Zarli, B.; Graziani, R.; Forsellini, E.; Croatto, U.; Bombieri, G. *J. Chem. Soc., Dalton Trans.* **1971**, 1501.
(52) Sutorik, A. C.; Kanatzidis, M. G. *J. Am. Chem. Soc.*, **1991**, *113*, 7754.
(53) Evans, W. J.; Miller, K. A.; Ziller, J. W.; DiPasquale, A. G.; Heroux, K. J.; Rheingold, A. L. *Organometallics* **2007**, *26*, 4287.

with soft-donor ligands are limited to $Pu(9\text{-ane}S_3)I_3(CH_3CN)_2$,[54] $Pu(tpza)I_3(CH_3CN)$,[54] $Pu(CH_3CN)_9[PF_6]_3$,[55] and $Pu(Et_2NCS_2)_4$.[56]

Finally, it is also worth mentioning that even taking into account the transition metals in addition to the f metals, examples of complete studies of the bonding of O, S, Se, and Te donor atoms to a metal are rare. However, in agreement with this study the general conclusions of those reports are broadly similar,[57−60] namely that M−O bonding contains a larger ionic component than do the M−E bonds for the heavier chalcogens, although there has been some debate as to the extent of $p\pi-d\pi$ interaction in the M−O bonds.

## 5. Conclusions

A systematic experimental and theoretical study of $M[(N(EPPh_2)_2)]_3$ (M = U, Pu, La, Ce; E = S, Se) and $M[N(EPiPr_2)_2]_3$ (M = U, Pu, La, Ce; E = S, Se, Te) and computational models has allowed us to provide some answers into two fundamental questions in f-element chemistry: (1) Is there more covalent contribution to actinide bonding with soft-donor atoms compared to lanthanide ions of similar ionic radius, and (2) do the bonding differences hold across the f-element series as the valence orbitals become increasingly contracted? We have shown that the U−E bonds are shorter than the corresponding La−E bonds to a significantly larger extent than the difference in the ionic radii between U(III) and La(III) and that the same is true between Pu(III) and Ce(III), consistent with increased covalency in actinide bonding. The magnitude of this difference is larger the "softer" the donor atom (Te > Se > S), again consistent with enhanced covalency. Natural, Mulliken, and molecular orbital analyses support the structural conclusions in finding greater covalency in the actinide complexes with the heavier chalcogen donors. The computational data indicate that the enhanced covalency in the Pu−E complexes as group 16 is descended is slightly less than that in the analogous U compounds, though it is still significant. We suggest that even as far along the actinide series as Am(III) and Cm(III), enhanced covalency over the corresponding lanthanide complexes may well play a role in industrially important 4f/5f separations that are an important component of proposed advanced nuclear fuel cycles.

**Acknowledgment.** We are grateful to the Heavy Element Chemistry Research Program, Chemical Sciences Division of the Office of Basic Energy Sciences, U.S. Department of Energy, and the G. T. Seaborg Institute at Los Alamos National Laboratory for funding. We thank the U.K. EPSRC for a Ph.D. studentship (to K.I.M.I.) and for computing resources under Grant GR/S06233. J.A.I. acknowledges DOE BES Grant No. ER15522. We also thank Dr. Iain May for useful discussions. We thank Anthony Mancino for the design of cover art and Maida Trujillo for help with graphics.

**Supporting Information Available:** CIF's, IR, UV/vis/near-IR, NMR spectra, and computational data. This material is available free of charge via the Internet at http://pubs.acs.org.

IC701618A

(54) Gaunt, A. J.; Matonic, J. H.; Scott, B. L.; Neu, M. P. In *Recent Advances in Actinide Science*; Alvarez, R., Bryan, N. D., May I., Eds.; Royal Society of Chemistry: Letchworth, U.K., 2006; p 183.
(55) Enriquez, A. E.; Matonic, J. H.; Scott, B. L.; Neu, M. P. *Chem. Commun. (Cambridge)* **2003**, 1892.
(56) Bagnall, K. W.; Brown, D.; Holah, D. G. *J. Chem. Soc. A* **1968**, 1149.
(57) Melnick, J. G.; Parkin, G. *Dalton Trans.* **2006**, 4207.
(58) Melnick, J. G.; Docrat, A.; Parkin, G. *Chem. Commun. (Cambridge)* **2004**, 2870.
(59) Hillier, A. C.; Liu, S.-Y.; Sella, A.; Elsegood, M. R. J. *Inorg. Chem.* **2000**, *39*, 2635.
(60) Howard, W. A.; Trnka, T. M.; Parkin, G. *Inorg. Chem.* **1995**, *34*, 5900.